Available online at www.sciencedirect.com

ScienceDirect

Procedia Structural Integrity 26 (2020) 293–298

Structural Integrity Procedia

www.elsevier.com/locate/procedia

The 1st Mediterranean Conference on Fracture and Structural Integrity, MedFract1

Ductile tearing of cryogenic valve components

Luigi Mario Viespoli[a,*], Pål Idar Ingebo[b], Filippo Berto[a]

[a]*Department of Mechanical and Industrial Engineering, Norwegian University of Science and Technology (NTNU), Richard Birkelands vei 2b, 7046 Trondheim, Norway*

[b]*Westad Industry AS, Heggenveien 530, 3360 Geithus, Norway*

Abstract

The paper reports the result of an experimental investigation on the torsional failure mechanics of the rotating components of a cryogenic valve. The rotating assembly is composed of an AISI 316L shaft connected by two cold drawn pins of the same alloy to a disc made of cast CF3M stainless steel. The shaft presents a notch, in the region lying outside the pressure boundary, which has the scope of reducing the maximum torque that this can withstand in case of torsional overload, making so that the region within the pressure boundary is not damaged. Different notch designs are tested to failure in pure torsion in order to estimate the ideal geometry to guarantee this condition to be met. The results have then been used for the calibration of a shear damage material model, useful to explore different designs. Also, the shaft-disc connection has been tested, presenting a resistance superior to that of the shaft. Such condition is representative of an ideal design for safe operation.

Keywords: Ductile fracture; notch; torsion; valve; stainless steel.

1. Introduction

High performance hydraulic butterfly valves are a fundamental part in piping for the oil & gas industry. These valves are constituted by an automatic or manually operated actuation system which transfers the torque to the "butterfly" disc through a shaft connected to it through locking pins, all enclosed in a cast case. They are built in

* Corresponding author.
E-mail address: luigi.m.viespoli@ntnu.no

10.1016/j.prostr.2020.06.037

standard size ranges, that is the disc diameter, between 80 and 1000 mm. Depending on the product, they can operate in ranges of temperature between -200 and +450 ºC and pressures generally up to 50 bar. To operate safely at low temperature and protect from environmental attacks, materials such as ductile austenitic stainless steels or titanium alloys are generally used for the production of their main components. These valves must respect the safety requirements provided by the API Standard 609 for the use in the Norwegian market, which imposes the imposes the resistance of all parts of the shaft and its connection to the disc to exceed by at least 10% the torsional static resistance of the components laying outside the pressure boundary. To ensure this condition is met the strength shall be determined by either calculation or testing. The scope of this work is to test the shaft and the shaft disc connection to ductile tearing under torsional loading for verifying the compliance to the standard and calibrating a material model for the evaluation of different feasible shaft designs. Derpeński (2019) studied the ductile fracture behaviour of aluminium under different loading conditions and with different notch geometries, finding that the notch radius has, under pure torsional load, an impact on the rotation to failure, but a limited influence on the torque to failure. Li et al. (2017) found how different levels of strain hardening impact the yield stress of 316L, but have a modest influence on the ultimate strength. The same alloy was tested by Czarkowski et al. (2011) at room and low temperature, at which the tensile properties were noticeably improved both in terms of strength and elongation to failure in annealed and hydrostatic extruded conditions. The notch influence on triaxiality and, consequently, failure location and mechanics for 316L was investigated by Peng et al. (2019). Numerous works are available in the literature on the influence of stress state on the plastic deformation and failure of metallic alloys, as those by Ribeiro et al. (2016), Wenchao et al. (2016) and Lou et al. (2014), but the case of shear failure induced by torsional loading remains underrepresented.

2. Stem testing

The shaft controlling the rotation on the disc for the valve model under examination is characterized by a diameter of 20 mm and a notch, see figure 1, in the area outside the pressure boundary is practiced to reduce the torsional resistance by at least 10% compared to the rest of the shaft. The alloy used for the production of these components is the AISI 316L austenitic stainless steel. A series of torsional static tests on the shaft's alloy were performed on specimens consisting of three different geometries: one reproducing the original notch, one characterized by a blunt notch and a third characterized by negligible stress intensification, see figure 1, with specimens having the same minimum cross section of a diameter of 17 mm. Two specimens for each geometry were tested. In addition, two tensile specimens, see figure 1, were tested to verify the nominal resistance stated by the material's supplier. An MTS servohydraulic multiaxial testing machine equipped with a 250 kN load cell and able to transfer a maximum torque of 4000 Nm. The result of the tensile test is a nominal stress Rm=680 MPa, see figure 2a, thus slightly exceeding the expected resistance for the alloy in question according to the supplier. The results for the torsional testing are summarized for the full range of rotation in figure 1b. The maximum range of rotation of the clamp is of 90º. For total rotation greater than this value the specimen has been unloaded, the clamp rotated back to the initial position and the test continued, explaining the non-continuous aspect of the torque-displacement curve for the low intensification (LI) specimen in figure 2b. This specimen experiences yielding soon after 500 Nm and sustains about 550º degrees of torsion before a ductile fracture in the central section is initiated and quickly propagates in a controlled way towards the centre of the section. The original notch (ON) and blunt notch (BN) present a higher torque, but a rotation noticeably smaller than LI. The region of interest of the plot is represented in figure 2c. ON and BN's torque-rotation curves are similar in the initial elastic-plastic trait, with a torque superior to that of LI due to a greater average cross section and to a more pronounced notch strengthening effect. The greater stress concentration induced by the small fillet radius of ON initiates the fracture earlier compared to BN, after 50º rather than 90º degrees of rotation as for the BN specimen. Also, in these two cases the propagation of the fracture is stable and the resisting torque of the specimen is progressively reduced with further rotation. The range of rotation up to 90º is of practical interest in case of overload because it corresponds with the rotation that can be imposed by the actuation system. Figure 3 summarizes the morphologies of the fractures for the specimens tested. TS, figure 3a, present the classic cup-cone morphology with ductile fracture by void nucleation in the central section and a 45º shear final fracture ring on the outer region, as typical for ductile metals. The reduction of area measured is 75%. The fractures for ON, BN and LI are reported in figures 3b, c and d and are, beyond the residual plastic twisting, similar to each other: a mode III shear fracture nucleated at the outer surface of the minimum cross section and propagated in the plane orthogonal to the torque direction, that is the specimen's axis.

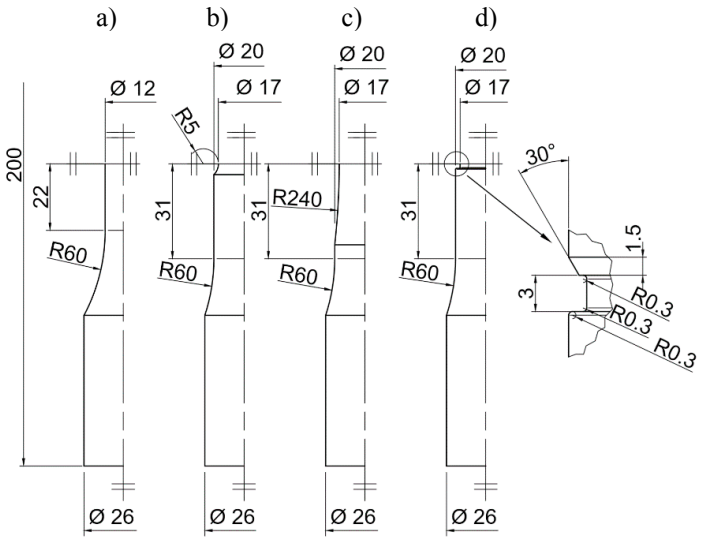

Fig. 1. (a) Tensile specimen geometry (TS); Torsional specimen geometries: (b) blunt notch (BN), (c) low intensification (LI), (d) original notch (ON).

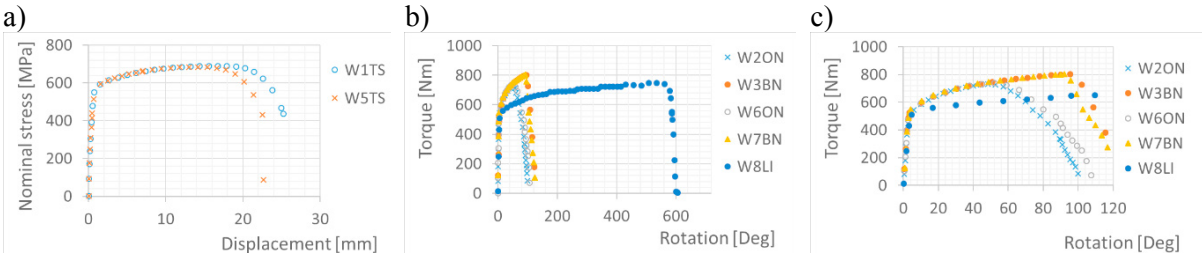

Fig. 2. (a) Testing results: tensile tests; (b) torsional tests; (c) torsional tests; focus on the rotation range of interest (c).

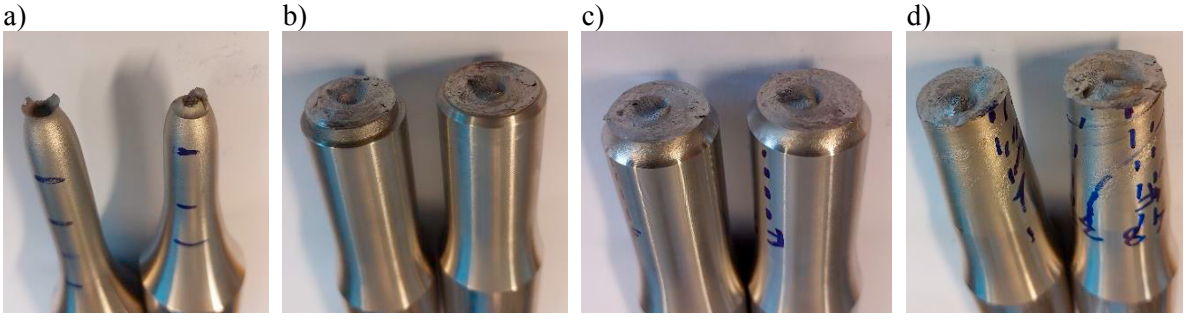

Fig. 3. Fracture morphologies: (a) tensile specimen; torsional specimens (b) ON, (c) BN, (d) LI.

3. Damage modelling

Part of the scope of this study is the calibration of a ductile damage model for the prediction of the torque response of different shafts and, in particular, shaft notch designs. The tool used for this purpose was the modelling of the specimens in Abaqus FEA environment and the solution of a built-in shear damage initiation and evolution material model with an explicit scheme. The explicit scheme is preferred because it is stable provided that the iteration time, depending on the speed of sound and the smallest element size, is short enough.

Any damage material model requires, beyond the mass and elastic-plastic properties, two sets of inputs: those relative to the damage initiation criterion and those relative to the damage evolution. The damage initiation is defined in the form of a shear stress which is dependent on the strain rate and on the shear stress ratio. The shear stress ratio is defined in the following way according to the Abaqus documentation:

$$\theta_S = \frac{q + k_S \cdot p}{\tau_{\max}} \tag{1}$$

Where:

q is the Von Mises equivalent stress;

$\tau_{\max}$ is the maximum shear stress, or half the Tresca equivalent stress;

p is the hydrostatic pressure;

k_S is a material parameter quantifying the influence of the hydrostatic pressure on the strain to failure.

The damage evolution is then defined as a progressive reduction of the stiffness of the elements with further deformation, in the form:

$$\underline{\sigma} = (1 - D) \cdot \underline{\bar{\sigma}} \tag{2}$$

Where:

$\underline{\sigma}$ is the stress tensor;

$\underline{\bar{\sigma}}$ is the stress tensor of the undamaged material;

D is the damage parameter.

The damage evolution criterion chosen for the analysis is energy based, with linear degradation. The use of the fracture energy for surface unit as input for the evolution reduces the mesh size sensitivity of the model. The mesh size is, for this kind of models, a parameter in itself: not a true material parameter, but one to which the set of values describing the damage evolution is strictly related. The modelling performed in this study used a coarse mesh, characterized by linear 8 nodes brick elements of 3 mm of side. As for ks, a value of 0.3 was used as generally adequate for ductile metals, Hooputra et al. (2004). The set of material properties which have given the best fitting of the experimental curves for the torsional tests on the ON, BN and LI specimens are reported in table 1. Figure 4a and 4b report the comparison between the tests' and the FEM results, which are in good agreement under a practical viewpoint. Figure 4c reports the evolution of the shear stress ratio with the clamp rotation. This has a value of approximately 1.75 and is the same for all the tests, since the shape of the notch does not influence it in a meaningful way and all tests were performed with no axial load. As a direct consequence, the parameters in table 1 are not a full material damage characterization, but suitable for the case of notched shafts in simple torsion.

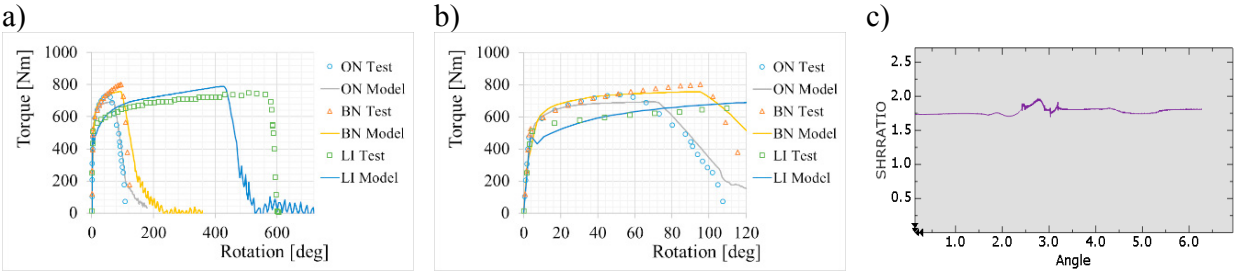

Fig. 4. Finite element damage model results over: (a) full range of rotation; (b) range of rotation of practical interest. (c) Evolution of the shear.

Table 1. Material model data.

Plastic table		**Elastic properties**		
Yield Stress [MPa]	Plastic Strain	Young's Modulus [MPa]	Poisson's Ratio	
560	0	193000	0.3	
800	0.07	**Density** [ton/mm^3]		
860	0.13	7.8E-9		
900	0.2	**Shear damage**		
940	0.36	Fracture Strain	Shear Stress Ratio	Fracture Energy [Nmm/mm^2]
1000	10	1.5	1.75	1600

4. Assembly testing

To check the compliance of the design to the API Standard 609 is was necessary to evaluate the resistance of the connection between shaft and disc. This connection is guaranteed by a transversal cut in the shaft which hosts two cold drawn AISI 316 steel pins passing through two holes in the disc each and axially fixed to the disc by a weld spot. To test the assembly a fixture was designed and manufactured, see figure 5a. In figure 5a we distinguish the clamps (a), the fixture (b), the shaft (c), the disc (d) and the pins' location (e). This fixture is held in the lower clamp of the testing machine and hosts the short end of the shaft, while the flat vertical surface transfers torque to the disc in the same direction (arrow in fig 5b) it would be transferred in case of system lock due to an intruding object or actuation system failure, figure 5b, for a maximum rotation of 90º. Three specimens of the assembly were tested, two with a free length of the shaft of 100 mm and a third with a shorter shaft, with a free length of 35 mm. The discs were produced in cast CF3M stainless steel, while the shafts in this case were manufactured from a S31803 duplex steel. The torque-rotation diagrams for these three tests are reported in figure 5c. During the first test, on long shaft, some slippage in the grip occurred due to low clamp oil pressure. The test was restarted from zero position, but the hardening occurred explains the deviation of the second run from the other two tests. The second test, on long shaft as well, follows an analogous trajectory, with the assembly not showing signs of failure for the full range of rotation and up to a torque of 1160 Nm. The third test, being on short shaft, is characterized by a higher twist for the same maximum rotation of 90º. This has a slight effect on the slope of the plastic part of the curve and two small torque drops after 75 and 80º of grip rotation. Observing figure 6b it's possible to notice how these small torque drops correspond to the failure of the weld spots locking the pins in place, while the structure is only slightly deformed. A small plastic deformation of the disc structure holding the pins is observed also for the long shaft specimens, figure 6a., while the shaft is bent due to the asymmetric application of the force generating the torque. In every case the shaft-disc connection structure resisted to a maximum torque just shy of 1200 Nm, well enough for respecting the safety standard with the maximum torque transferrable by the 20 mm in diameter AISI 316L shafts.

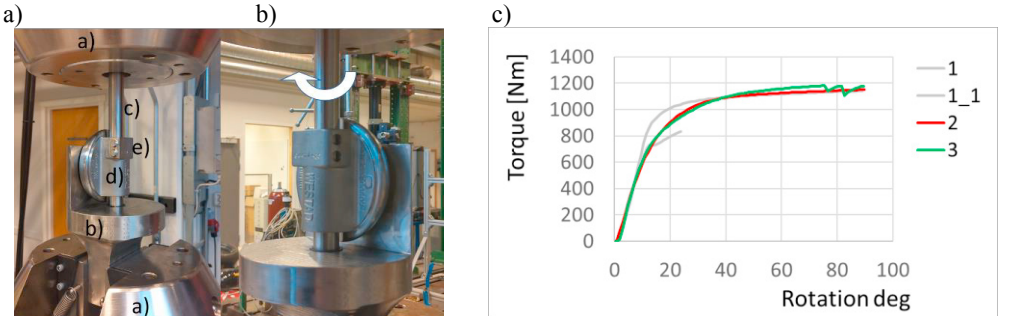

Fig. 5. (a) first picture; (b) second picture.

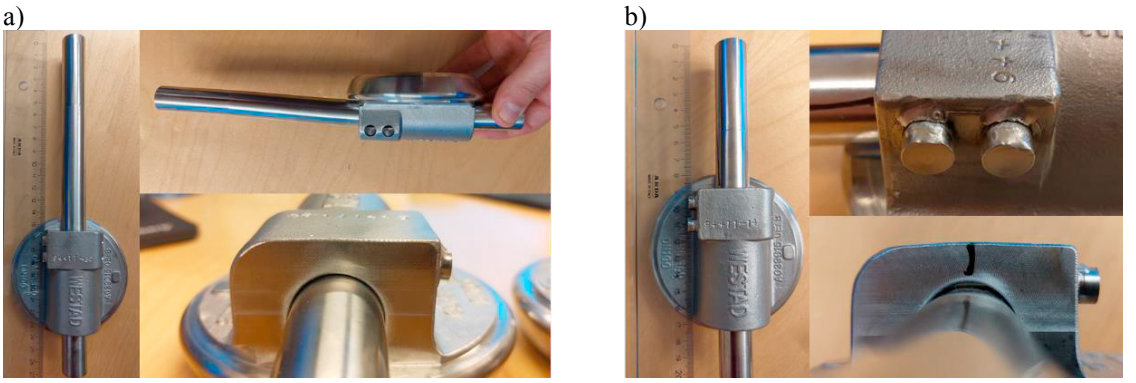

Fig. 6. (a) first picture; (b) second picture.

5. Conclusions and further developments

Specimens of different geometries have been subjected to tensile and torsional static testing to characterize the static failure behaviour of the alloy used for the production of hydraulic valve shafts and a finite element ductile failure model has been calibrated on the base of the results. To verify the compliance with the API Standard 609, the shaft-disc connection resistance to torsional load was tested using a custom-built fixture. The main conclusions of the work are:

- The results obtained for the disc design tested are satisfactory: the connection is strong enough to survive an overload of the system and respect the API Standard 609.
- The stem shear damage material model is effective for high strains even with coarse mesh.
- The geometry of the notch influences the rotation to failure, but does not have a heavy influence on the torque.

References

http://www.westad.com/

API Std 609

Derpeński Ł., 2019. Ductile fracture behaviour of notched aluminium alloy specimens under complex non-proportional load. Materials, 12(10):1598.

Li K., Peng J., 2017. Mechanical behaviour of 316L stainless steel after strain hardening. MATEC Web Conf. 114 02003.

Czarkowski P., Krawczynska A.T., Slesinski R., Brynk T., Budniak J., Lewandowska M., Kurzydlowski K.J., 2011. Low temperature mechanical properties of 316L type stainless steel after hydrostatic extrusion. Fusion Engineering and Design, 86(9–11), 2517-2521.

Peng, J., Wang, Y., Dai, Q., Liu, X., Liu, L., Zhang, Z., 2019. Effect of stress triaxiality on plastic damage evolution and failure mode for 316L notched specimen. Metals, 9, 1067.

Zhang X.W., Wen J.F., Zhang X.C., Wang X.G., Tu S.T., 2019. Effects of the stress state on plastic deformation and ductile failure: Experiment and numerical simulation using a newly designed tension□ shear specimen. Fatigue Fract Eng Mater Struct, 42: 2079– 2092.

Ribeiro J., Santiago A., Rigueiro C., 2016. Damage model calibration and application for S355 steel. Procedia Structural Integrity, 2, 656-663.

Li W., Liao F., Zhou T., Askes H., 2016. Ductile fracture of Q460 steel: Effects of stress triaxiality and Lode angle. Journal of Constructional Steel Research, Volume 123, Pages 1-17.

Lou Y., Yoon J. and Huh H., 2014. Modelling of shear ductile fracture considering a changeable cut-off value for stress triaxiality. NUMISHEET 2014: Proceedings of the 9th International Conference and Workshop on Numerical Simulation 3D Sheet Metal Forming Processes, AIP Publishing, Melville, N.Y., pp. 567-570.

Abaqus Documentation 6.14

Hooputra H., Gese H., Dell H., Werner H., 2004. A comprehensive failure model for crashworthiness simulation of aluminium extrusions. International Journal of Crashworthiness, vol. 9, no. 5, pp. 449–464.